Uniform chemical pressure effect in solid solutions $Ba_{1-x}Sr_xFe_2As_2$ and $Sr_{1-x}Ca_xFe_2As_2$

S. R. Saha, K. Kirshenbaum, N. P. Butch, and J. Paglione

Center for Nanophysics and Advanced Materials, Department of Physics, University of Maryland, College Park, MD 20742, USA.

P. Y. Zavalij

Department of Chemistry and Biochemistry, University of Maryland, College Park, MD 20742

E-mail: paglione@umd.edu

Abstract.
The effect of alkaline earth substitution on structural parameters was studied in high-quality single crystals of $Ba_{1-x}Sr_xFe_2As_2$ and $Sr_{1-x}Ca_xFe_2As_2$ grown by the self-flux method. The results of single-crystal and powder x-ray diffraction measurements suggest a continuous monotonic decrease of both a- and c-axis lattice parameters, the c/a tetragonal ratio, and the unit cell volume with decreasing alkaline earth atomic radius as expected by Vegard's law. As a result, the system experiences a continuously increasing chemical pressure effect in traversing the phase diagram from $x = 0$ in $Ba_{1-x}Sr_xFe_2As_2$ to $x = 1$ in $Sr_{1-x}Ca_xFe_2As_2$.

The recent discovery of high-temperature superconductivity in iron-based compounds has attracted much interest. The parent phases of these compounds generally show antiferromagnetic order that onsets between 130 K and 200 K, with superconductivity emerging when the antiferromagnetic order of the parent compounds is suppressed [1, 2, 3, 4, 5]. This proximity of magnetic and superconducting order parameters is widely thought to be a key argument for an unconventional pairing mechanism, likely mediated by spin fluctuations [6, 7] similar to the cuprates [8, 9]. But in strong contrast to the copper oxides, superconductivity in iron arsenides can be induced without changing the carrier concentration, either by applying external pressure [10, 11] or by isovalent chemical substitution. The highest T_c achieved so far in these materials is ~ 55 K in $SmO_{1-x}F_xFeAs$ [5] and (Sr,Ca)FeAsF [12, 13]. Oxygen-free FeAs-based compounds with the $ThCr_2Si_2$-type (122) structure also exhibit superconductivity induced by chemical substitution of alkali or transition metal ions [3, 14, 15, 16], the application of large pressures [11, 17, 18, 19], or lattice strain [20], with transition temperatures as high as ~ 37 K.

For the 122 phase, superconductivity has been induced by substituting Fe with not only $3d$-transition metals such as Co and Ni, but also some of the $4d$- and $5d$-transition metals. Recently, Ru, Ir, and Pt substitution for Fe were also shown to induce superconductivity in $SrFe_2As_2$ and $BaFe_2As_2$ [21, 22, 23]. Superconductivity with $T_c\sim 31$ K has also been shown to occur by isovalent substitution of P for As [24]. This gives the opportunity to tune magnetic character without nominally changing charge carrier concentrations, for instance making the interpretation of transport coefficients much simpler than in the case of charge doping.

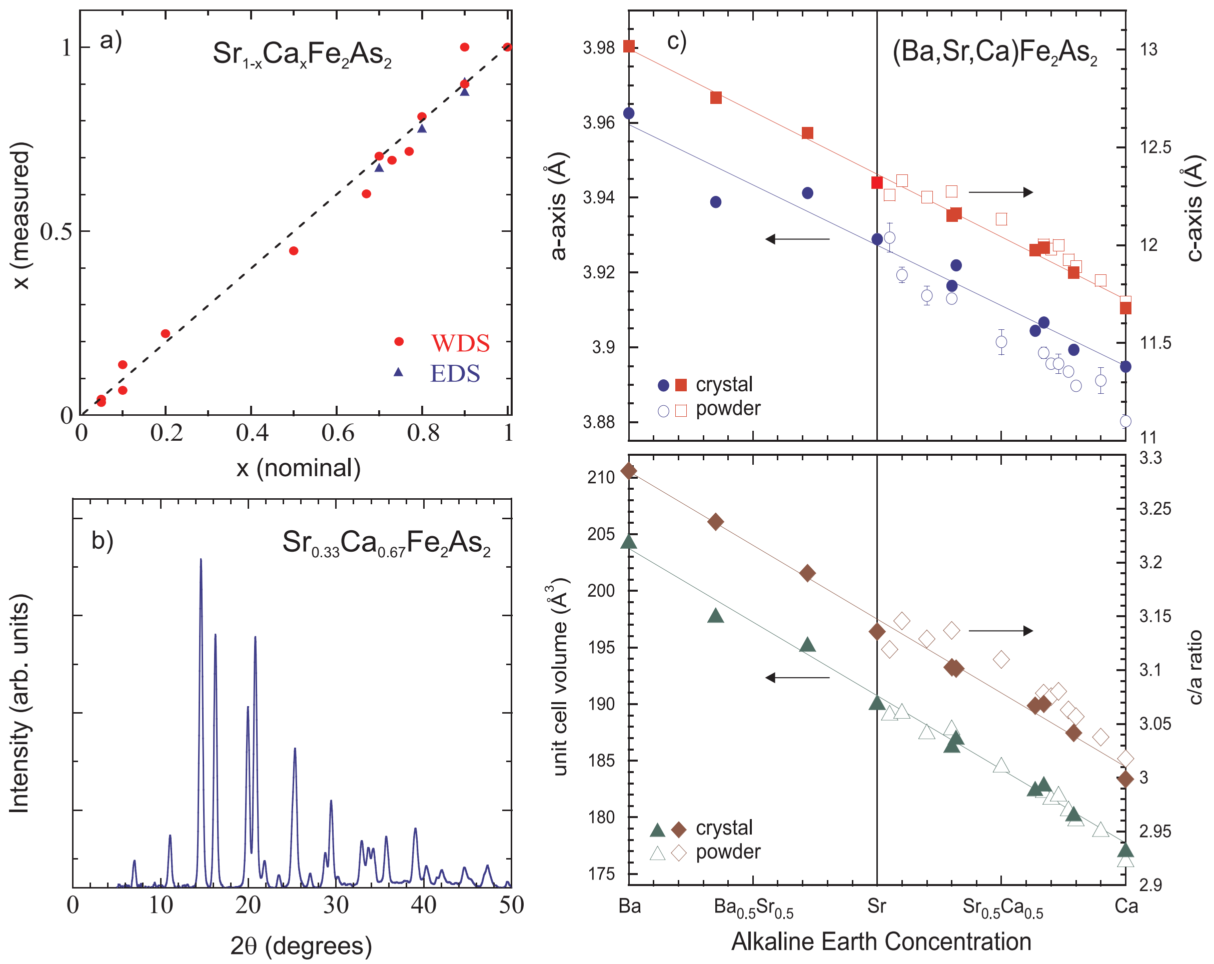

Figure 1. (a) Measured Ca concentration of $Sr_{1-x}Ca_xFe_2As_2$ single-crystal samples as a function of nominal concentration x, as determined by wavelength dispersive x-ray spectroscopy (data points represent an average value of 8 scanned points for each concentration). Some of the specimens are also confirmed by energy dispersive X-ray spectroscopy (EDS). The dotted line is a guide to eye which traces x(measured)=x(nominal). (b) Typical x-ray powder diffraction pattern, shown for sample $Sr_{0.33}Ca_{0.67}Fe_2As_2$, obtained by using Mo-$K_\alpha$ radiation. The main peaks can be indexed with a tetragonal structure and there are no impurity phases detected within experimental accuracy. (c) Upper panel: Variation of the a- and c-axis lattice constants as a function of alkaline earth substitution in the series $Ba_{1-x}Sr_xFe_2As_2$ (left half) and $Sr_{1-x}Ca_xFe_2As_2$ (right half) as determined from single crystal x-ray diffraction measurements at 250 K of single-crystal samples. Corresponding c/a ratio and the unit cell volume are plotted in the lower panel. In both panels, solid symbols indicate data acquired using single-crystal specimens and open symbols represent data determined by powder x-ray diffraction.

In order to investigate the possibility of applying uniform chemical pressure in a continuous manner, we have synthesized the series of solid solutions $Ba_{1-x}Sr_xFe_2As_2$ and $Sr_{1-x}Ca_xFe_2As_2$ by substituting isovalent alkaline earth atoms, and investigated the evolution of the crystal structure by high-resolution powder and single-crystal x-ray diffraction. Here we present our preliminary results that suggest the unit cell of the Ba-Sr-Ca substitution series experiences a monotonic uniform chemical pressure as a function of alkaline earth atomic radius.

Single-crystal samples of $Ba_{1-x}Sr_xFe_2As_2$ and $Sr_{1-x}Ca_xFe_2As_2$ were grown using the FeAs self-flux method [20]. Fe was first separately pre-reacted with As via solid-state reaction of Fe (99.999%) powder with As (99.99%) powders in a quartz tube of partial atmospheric pressure of Ar. The precursor materials were mixed with elemental Sr (99.95%) with either Ba (99.95%) or Ca (99.95%) in the ratio 4:1$-x$: x, placed in an alumina crucible and sealed in a quartz tube under partial Ar pressure. The mixture was heated to 1150°C, slow-cooled to a lower temperature and then quenched to room temperature. Typical dimensions of as-grown single crystal specimen are $\sim$100 μm thickness and up to 5 mm width. Chemical analysis was performed using both energy- and wavelength-dispersive x-ray spectroscopy (WDS).

Both EDS and WDS analysis of all $Ba_{1-x}Sr_xFe_2As_2$ and $Sr_{1-x}Ca_xFe_2As_2$ samples showed the proper 1:2:2 stoichiometry in all specimens reported herein, with no indication of impurity phases. Figure 1(a) compares the nominal alkaline earth concentration x in $Sr_{1-x}Ca_xFe_2As_2$ crystals with that measured by WDS and EDS analysis, using an average value determined from 8 different spots on each specimen. As shown by the dotted line guide, the actual concentrations found by WDS are equal to the nominal values of x to within experimental error, indicating homogeneous substitution in this series of solid solutions.

Diffraction patterns were obtained by both powder and single-crystal x-ray diffraction and Rietfeld refinement (SHELXS-97) to $I4/mmm$ structure. Powder x-ray diffraction was performed at 250 K using a Smart Apex2 diffractometer with Mo-K_α radiation and a graphite monochromator. Figure 1(b) shows a typical x-ray diffraction pattern obtained from a single-crystal sample of $Sr_{0.3}Ca_{0.7}Fe_2As_2$. All of the main peaks can be indexed to the $ThCr_2Si_2$ structure, with no impurity phases detected.

Table 1. Crystallographic data for $SrFe_2As_2$ and $Sr_{0.3}Ca_{0.7}Fe_2As_2$ determined by single-crystal x-ray diffraction at 250 K. The tetragonal structure was solved and refined using the SHELXS-97 software, yielding lattice constants with residual factor R= 1.36% and 1.95% for $SrFe_2As_2$ and $Sr_{0.33}Ca_{0.67}Fe_2As_2$, respectively.

	$SrFe_2As_2$	$Sr_{0.33}Ca_{0.67}Fe_2As_2$
Temperature	250 K	250 K
Space group	I4/mmm	I4/mmm
a(Å)=b(Å)	3.9289(3)	3.9066(8)
c(Å)	12.3172(12)	11.988(5)
V(Å^3)	190.17(4)	182.95(9)
Z	2	2
Density(g/cm^3)	6.098	6.045
Atomic parameters:		
Sr/Ca	2a(0,0,0)	2a(0,0,0)
Fe	4d(1/2,0,1/4)	4d(1/2,0,1/4)
As	4e(0,0,z)	4e(0,0,z)
	z=0.36035(5)	z=0.36423(7)
Atomic displacement parameters U_{eq} (Å^2):		
Sr1/Ca1	0.0108(2)	0.0116(5)
Fe1	0.0096(2)	0.0125(3)
As1	0.00964(17)	0.0119(2)
Bond lengths and angles:		
Sr/Ca-As (Å)	3.2677(4) × 8	3.2062(7) × 8
Fe-As (Å)	2.3890(4) × 4	2.3855(7) × 4
Fe-Fe (Å)	2.7782(2) × 4	2.7624(6) × 4
As-Fe-As(deg)	110.63(3) × 2	109.94(4) × 4
	108.896(14) × 4	109.24(2) × 4
Fe-As-Fe(deg)	71.105(14) × 4	70.76(2) × 4

Table 1 shows the crystallographic parameters determined by single-crystal x-ray-diffraction at 250 K in $Sr_{0.3}Ca_{0.7}Fe_2As_2$. A Bruker Smart Apex2 diffractometer with Mo-K_α radiation, a graphite monochromator with monocarp collimator, and a CCD area detector were used for this experiment. The structure was refined with SHELXL-97 software using 1033 measured reflections of which 115 were unique and 108 observed. The final residuals were R_1= 1.36% and 1.96% for the observed data and wR_2= 3.31% and 4.52% for all data for $SrFe_2As_2$ and $Sr_{0.3}Ca_{0.7}Fe_2As_2$ respectively. Sr and Ca atoms were found to reside in the same site with a refined Ca:Sr = 0.33(1):0.67(1), giving the exact formula $Sr_{0.33}Ca_{0.67}Fe_2As_2$ from x-ray analysis.

Figure 1(c) presents the variation of the a- and c-axis lattice constants (upper panel), the unit cell volume and the tetragonal c/a ratio (lower panel) with Ba-Sr and Sr-Ca concentrations determined from refinements of the single crystal x-ray diffraction data for $Ba_{1-x}Sr_xFe_2As_2$ and $Sr_{1-x}Ca_xFe_2As_2$ crystals taken at 250 K. Within experimental accuracy, the a- and c-axis lattice constants, the c/a ratio, and the unit cell volume all show a monotonic linear decrease with alkaline earth substitution in the continuous series from $BaFe_2As_2$ to $SrFe_2As_2$ to $CaFe_2As_2$. This fact indicates that the whole (Ba,Sr,Ca)Fe_2As_2 series progression experiences a uniform chemical pressure effect due to the reduction of the cation size that follows Vegard's law, as expected for the decreasing ionic radii of Ba, Sr and Ca, respectively.

The lattice parameters of $Ba_{1-x}Sr_xFe_2As_2$ obtained in our experiments are consistent with the data reported in a recent study [25, 26], which found a systematic increase of T_0 with increasing Sr content and no superconductivity. On the other hand, substitution of arsenic for the smaller phosphorus atoms, also instituting a chemical pressure effect, induces superconductivity in $BaFe_2As_{2-x}P_x$ [25]. Thus, a pressure-volume effect is clearly an oversimplified explanation for superconductivity in $BaFe_2As_{2-x}P_x$. In the future, it will be interesting to investigate the evolution of superconductivity combining both the chemical pressure effect of alkaline earth substitution studied here and another tuning parameter that induces superconductivity in order to investigate the role of lattice density in these phenomena.

References

[1] Kamihara Y, Watanabe T, Hirano M., and Hosono H., J. Am. Chem. Soc. 130, 3296 (2008).
[2] Cruz de la C *et al.*, 2008 *Nature* **453**, 899.
[3] Rotter M, Tegel M, and Johrendt D, 2008 *Phys. Rev. Lett.* **101** 107006.
[4] Saha S R, Butch N P, Kirshenbaum K, and Paglione Johnpierre, 2009 *Phys. Rev. B* **79** 224519.
[5] Ren Z -A *et al.*, 2008 *Chin. Phys. Lett.* **25** 2215.
[6] Mazin I I, Schmalian J, 2009 *Physica C* **469** 614.
[7] Christianson A D *et al.*, 2008 *Nature* **456**, 930.
[8] Shirane G *et al.*, 1987 *Phys. Rev. Lett.* **59** 1613.
[9] Keimer B *et al.*, 1992 *Phys. Rev. B* **46**, 14034.
[10] Okada H *et al.*, 2008 *J. Phys. Soc. Jpn.* **77** 113712.
[11] Alireza P L *et al.*, 2009 *J. Phys.: Condens. Matt.* **21**, 012208.
[12] Zhu X *et al.*, 2009 *Europhys. Lett.* **85** 17011.
[13] Cheng P *et al.*, 2009 *Euro Phys. Lett.* **85** 67003.
[14] Sasmal K *et al.*, 2008 *Phys. Rev. Lett.* **101** 107007.
[15] Sefat A S, Jin R, McGuire M A, Sales B C, Singh D J, and Mandrus D, 2008 *Phys. Rev. Lett.* **101** 117004.
[16] Leithe-Jasper A, Schnelle W, Geibel C, and Rosner H, 2008 *Phys. Rev. Lett.* **101** 207004.
[17] Torikachvili M S, Bud'ko S L, Ni N, and Canfield P C, 2008 *Phys. Rev. Lett.* **101** 057006.
[18] Park T *et al.*, 2008 *J. Phys.: Condens. Matt.* **20** 322204.
[19] Kumar M *et al.*, 2008 *Phys. Rev. B* **78** 184516.
[20] Saha S R, Butch N P, Kirshenbaum K, and Paglione J., 2009 *Phys. Rev. Lett.*, **103** 037005.
[21] Schnelle W *et al.*, 2009 *Phys. Rev. B* **79** 214516.
[22] Han F *et al.*, 2009 *Phys. Rev. B.* **80** 024506.
[23] Saha S R *et al.*, 2010 *J. Phys. Condens. Matt.*, **22** 072204.
[24] Kasahara S *et al.*, 2010 *Phys. Rev. B* **81** 184519.
[25] Wang Z, Yang H, Ma C, Tian H, Shi H, Lu J, Zeng L, Li J, 2009 *J. Phys. Condens. Matt.*, **21** 495701.
[26] Rotter M, Hieke C, Johrendt D, 2010 *Phys. Rev. B* **82** 014513.